AD-A121 481 WHAP A FINITE ELEMENT COMPUTER CODE FOR THE STRUCTURAL 1/1
ANALYSIS OF AXISYM.. (U) NAVAL WEAPONS CENTER CHINA LAKE
CA J C SCHULZ OCT 82 NWC-TP-6369

UNCLASSIFIED F/G 9/2 NL

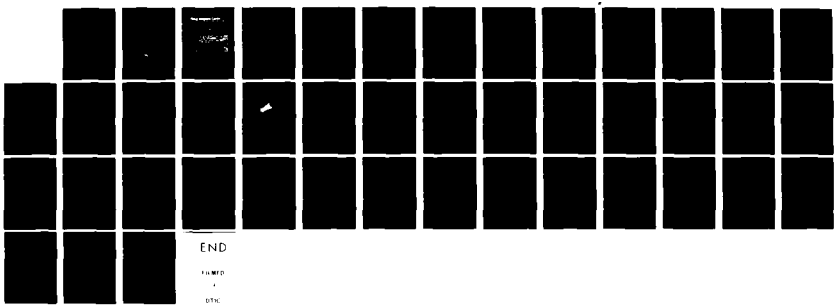

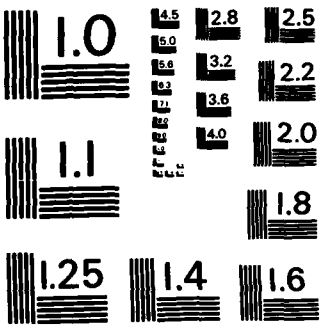

NWC TP 6369

(12)

WHAP, A Finite Element Computer Code for the Structural Analysis of Axisymmetric Warheads Impacting Targets at Obliquity

by
Jan C. Schulz
Research Department

OCTOBER 1982

NAVAL WEAPONS CENTER
CHINA LAKE, CALIFORNIA 93555

Approved for public release; distribution unlimited.

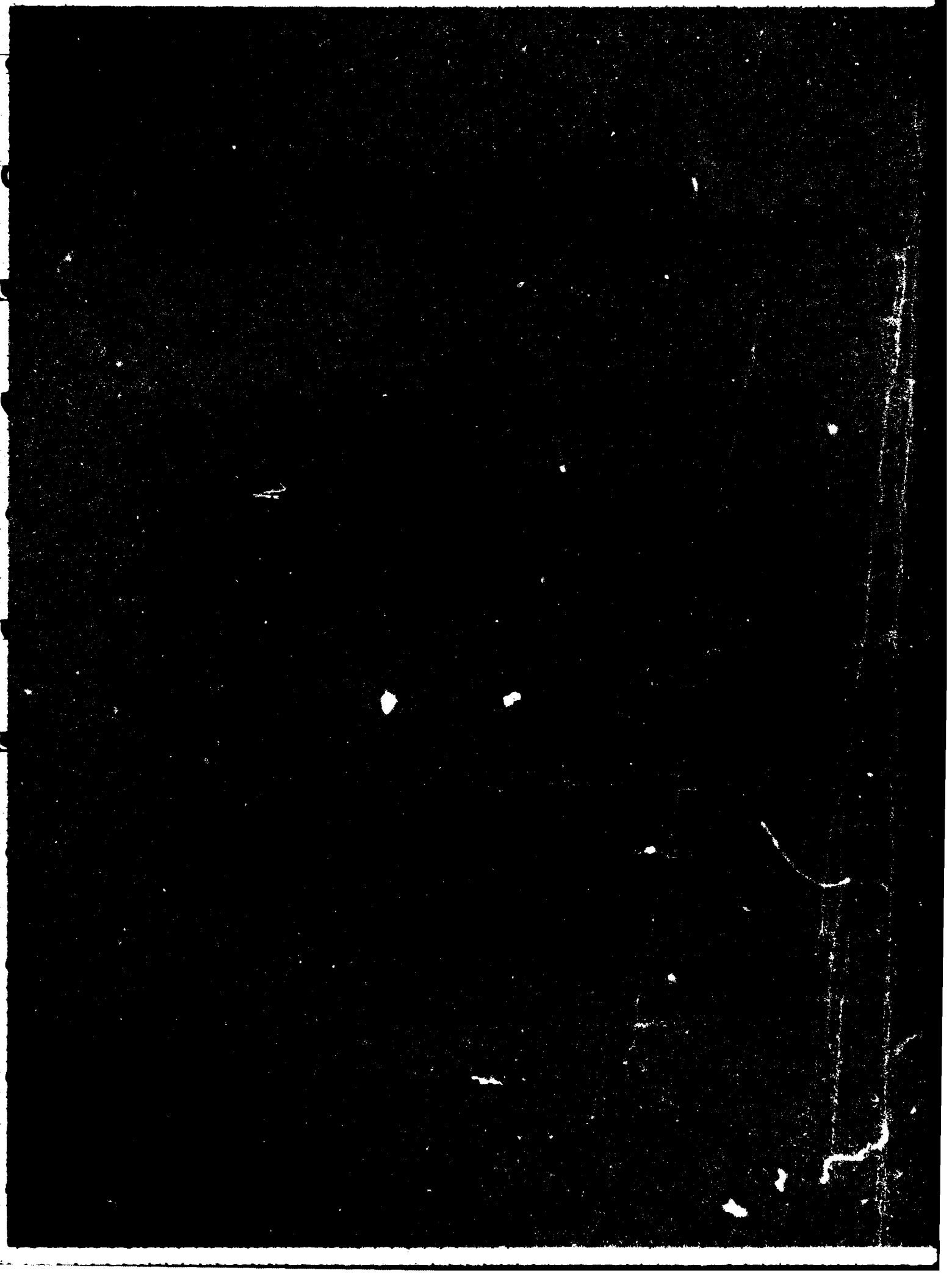

UNCLASSIFIED

SECURITY CLASSIFICATION OF THIS PAGE *(When Data Entered)*

REPORT DOCUMENTATION PAGE		READ INSTRUCTIONS BEFORE COMPLETING FORM
1. REPORT NUMBER NWC TP 6369	2. GOVT ACCESSION NO. AD-A122 482	3. RECIPIENT'S CATALOG NUMBER
4. TITLE *(and Subtitle)* WHAP, A FINITE ELEMENT COMPUTER CODE FOR THE STRUCTURAL ANALYSIS OF AXISYMMETRIC WARHEADS IMPACTING TARGETS AT OBLIQUITY		5. TYPE OF REPORT & PERIOD COVERED Final Report Fiscal Years 1981 and 1982 6. PERFORMING ORG. REPORT NUMBER
7. AUTHOR*(s)* Jan C. Schulz		8. CONTRACT OR GRANT NUMBER*(s)*
9. PERFORMING ORGANIZATION NAME AND ADDRESS Naval Weapons Center China Lake, California 93555		10. PROGRAM ELEMENT, PROJECT, TASK AREA & WORK UNIT NUMBERS AIRTASK A03W-03P2/008B/2F32-300-000
11. CONTROLLING OFFICE NAME AND ADDRESS Naval Weapons Center China Lake, California 93555		12. REPORT DATE October 1982 13. NUMBER OF PAGES 40
14. MONITORING AGENCY NAME & ADDRESS*(if different from Controlling Office)*		15. SECURITY CLASS. *(of this report)* UNCLASSIFIED 15a. DECLASSIFICATION/DOWNGRADING SCHEDULE

16. DISTRIBUTION STATEMENT *(of this Report)*

Approved for public release; distribution unlimited

17. DISTRIBUTION STATEMENT *(of the abstract entered in Block 20, if different from Report)*

18. SUPPLEMENTARY NOTES

19. KEY WORDS *(Continue on reverse side if necessary and identify by block number)*

Finite Elements	Structural Analysis
HONDO II	Warheads
Impact	WHAP

20. ABSTRACT *(Continue on reverse side if necessary and identify by block number)*

See reverse side of this form.

DD FORM 1 JAN 73 1473 EDITION OF 1 NOV 65 IS OBSOLETE
S/N 0102-LF-014-6601

UNCLASSIFIED

SECURITY CLASSIFICATION OF THIS PAGE *(When Data Entered)*

(U) *WHAP, A Finite Element Computer Code for the Structural Analysis of Axisymmetric Warheads Impacting Targets at Obliquity*, by Jan C. Schulz. China Lake, Calif., Naval Weapons Center, October 1982. 40 pp. (NWC TP 6369, publication UNCLASSIFIED.)

(U) The development of a finite element computer code for the structural analysis of axisymmetric warheads impacting targets at obliquity is described. Called WHAP (for Warhead Analysis Program), this code is essentially an extension to three-dimensions of the HONDO II code. The theoretical basis for the code, its computer implementation, and its use to solve example problems are discussed. User instructions and other pertinent information are given in the appendixes.

CONTENTS

INTRODUCTION

Warheads impacting ships, concrete bunkers or other targets are often required to survive perforation or penetration in detonable condition to successfully complete their missions. The design of such warheads requires a knowledge of the stresses and deformations induced by impact from which an assessment of survivability can be made. Finite element structural analysis procedures offer an attractive way of determining these quantities.

Analyses of warheads impacting targets at normal obliquity[1] have been performed at the Naval Weapons Center using the two-dimensional finite element code, HONDO II.[2] Analyses of warheads impacting targets at non-normal obliquity require a full three-dimensional treatment and can be extremely expensive using currently available codes.

This report documents the development of a three-dimensional finite element code for the analysis of axisymmetric warheads impacting targets at obliquity. The aim of this effort was to produce a specialized and efficient code well-adapted to the Naval Weapons Center computer system (UNIVAC 1100/82) and capable of providing useful information to the warhead designer at a reasonable cost. In addition, it was hoped to make the new code as compatible as possible with locally written pre- and post-processors for the HONDO II program to minimize the extra effort required for oblique impact analyses.

For presentation purposes this work can be divided into three parts:

1. Finite element theory.
2. Computer implementation of theory; i.e., writing and checkout of code.
3. Employment of the code in the solution of a realistic projectile impact problem.

---

[1] J. C. Schulz. "Finite Element Analysis of a Kinetic Energy Warhead Penetrating Concrete," in *Proceedings of the 4th International Symposium on Ballistics, Monterey, California, October 1978.* Washington, D.C., American Defense Preparedness Association, 1978. (Publication UNCLASSIFIED.)

[2] Sandia Laboratories. *HONDO II, A Finite Element Computer Program for Large Deformation Dynamic Response of Axisymmetric Solids*, by S. W. Key, Z. E. Beisinger and R. D. Krieg. Albuquerque, N. Mex., October 1978. (SAND78-0422, publication UNCLASSIFIED.)

These are discussed in subsequent sections. User instructions and other pertinent information are given in appendixes.

FINITE ELEMENT THEORY

PROBLEM DESCRIPTION

A solid body of revolution generated by rotating a planar area around an axis is shown in Figure 1. Points in the body may be specified by rectangular cartesian coordinates (x_i; i = 1, 2, 3) or cylindrical coordinates (r, θ, z). Cylindrical coordinates will be used for convenience in data input, while rectangular cartesian coordinates will be used for the finite element solution.

At time t = 0, the initial coordinates of points in the body are (X_i) and the body is assumed to be strain-free. Subsequently, a normal pressure loading (not necessarily axisymmetric) may be applied resulting in traction components (S_i) acting over a portion of the surface, A_s. The body may also have an initial homogeneous motion such that all points have axial velocity components (0, 0, V_3) at t = 0. Displacement boundary conditions (limited to the setting of one or more displacement components equal to zero) may be specified over some region, A_d.

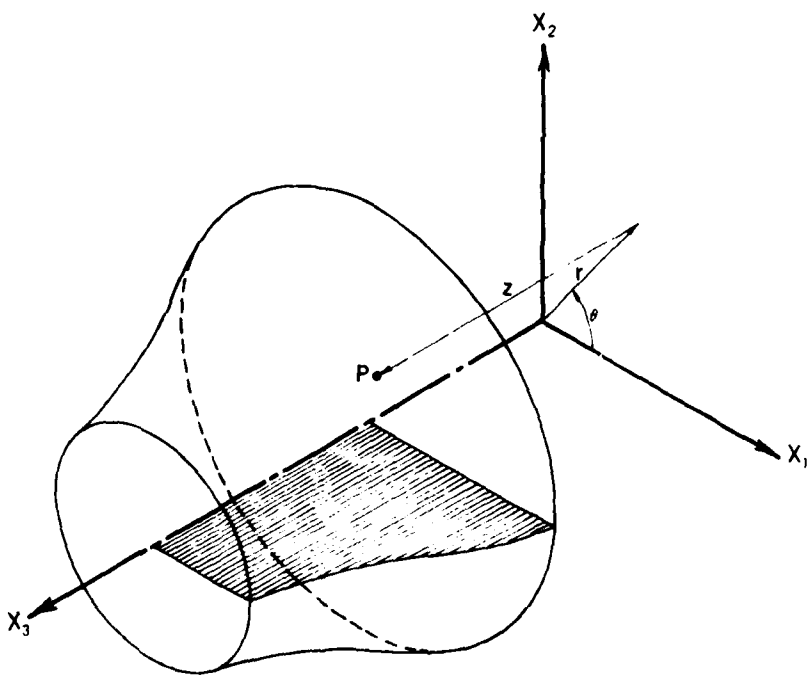

FIGURE 1. Solid Body of Revolution Showing Rectangular Cartesian and Cylindrical Coordinate Systems and Generating Plane.

As a result of the pressure loading and initial velocity and subject to the displacement boundary conditions, the body will undergo a motion

$$x_i = x_i(X_1, X_2, X_3, t) \tag{1}$$

after which it may no longer be axisymmetric. The problem is to determine the motion and to ascertain the displacement and stresses throughout the body as functions of time. An analytic solution is, of course, not feasible except in certain special cases, and some form of approximate solution is required. The finite element method is used to obtain such a solution.

STARTING POINT

A general three-dimensional theory for the large displacement, inelastic analysis of solid bodies subjected to impulsive loads is given by Key and then specialized to solids of revolution subjected to axisymmetric loads to form the basis for the HONDO II finite element code.[2] The same general theory is derived here; the only specialization being to a rectangular cartesian coordinate system.

FINITE ELEMENT IDEALIZATION

The generating planar area is subdivided into quadrilateral regions and then rotated around the axis to form a set of annular rings of quadrilateral cross section. The rings are cut by a series of radial planes. (Equal spacing of the planes in the circumferential direction is used in the computer implementation, although not required by the theory.) The body is thus divided into hexahedral elements as indicated in Figure 2.

A typical element, as shown in Figure 3, can be specified by its eight corner nodal points. By convention the numbering must be counterclockwise around the quadrilateral faces in consecutive radial planes. A local coordinate system is introduced so that the initial location of a typical point inside the element can be given in terms of its global coordinates (x_i) or its local coordinates (a_i). The transformation equations are

$$x_i = \sum_{j=1}^{8} x_{ij}\phi_j(a_1, a_2, a_3) \tag{2}$$

where (x_{ij}) are the initial global coordinates of the nodes (in the element numbering system) and $\phi_j(a_1, a_2, a_3)$ are shape functions defined by

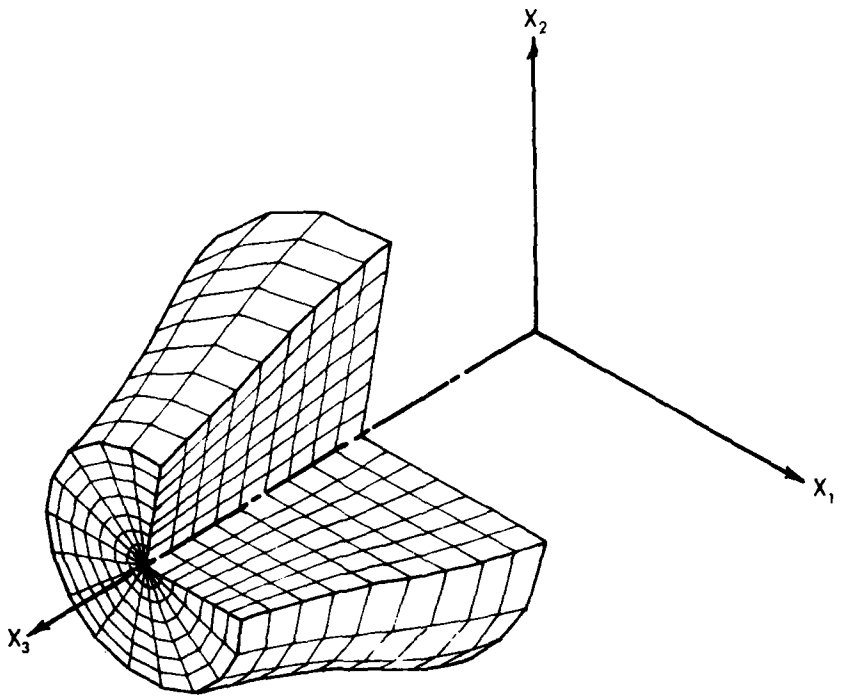

FIGURE 2. Solid of Revolution Partially Cut Away Showing Division Into Finite Elements.

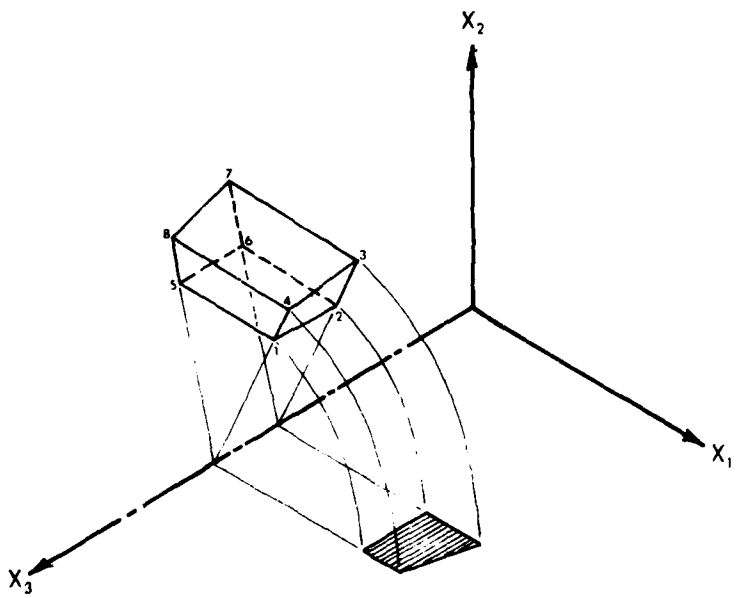

FIGURE 3. Typical Finite Element Showing Element Node Numbering Convention.

$$
\begin{aligned}
\phi_1 &= (1 - a_1)(1 - a_2)(1 - a_3)/8 \\
\phi_2 &= (1 + a_1)(1 - a_2)(1 - a_3)/8 \\
\phi_3 &= (1 + a_1)(1 + a_2)(1 - a_3)/8 \\
\phi_4 &= (1 - a_1)(1 + a_2)(1 - a_3)/8 \\
\phi_5 &= (1 - a_1)(1 - a_2)(1 + a_3)/8 \\
\phi_6 &= (1 + a_1)(1 - a_2)(1 + a_3)/8 \\
\phi_7 &= (1 + a_1)(1 + a_2)(1 + a_3)/8 \\
\phi_8 &= (1 - a_1)(1 + a_2)(1 + a_3)/8
\end{aligned} \tag{3}
$$

Subdivision of the body into elements and the introduction of local coordinates are matters of definition and involve no approximation (except at the surface of the body where the planar faces of the elements will not exactly fit the curved surface). At this point, however, the fundamental finite element idealization is made. The displaced positions of points inside the deformed element are approximated by

$$x_i = \sum_{j=1}^{8} x_{ij}\phi_j \tag{4}$$

where (x_{ij}) are the global coordinates of the nodes. With this approximation the number of degrees of freedom in the idealized body is reduced from an uncountable infinity to three times the number of nodes (unless displacement boundary conditions are imposed at some of the nodes). Displacement compatibility at the common faces of adjoining elements is maintained.

Equations 4 give the positions of points within any one element in terms of the positions of its nodes. A different set of equations must be written for each element. Equivalently, a single set of equations can be written which gives the positions of points throughout the entire body. Thus,

$$x_i = \sum_{j=1}^{N_p} x_{ij}\Phi_j \tag{5}$$

where N_p is the total number of nodal points in the body, (x_{ij}) are the coordinates of the jth node (in a global node numbering system rather than the element node numbering system of Equations 4) and Φ_j are the basis functions defined by:

$\Phi_j = 0$ in elements for which the jth node is not a corner node,
$\Phi_j = \phi_k$ in elements for which the jth node is a corner node, where k is the number of the jth node in the element node numbering system.

EQUATIONS OF MOTION

Equations of motion for the finite element model of the body can be obtained using the principle of virtual displacements. This principle requires that the differential form

$$\delta\pi = \int_V \rho \ddot{x}_i \delta x_i dV + \int_V \sigma_{im} \frac{\partial(\delta x_i)}{\partial x_m} dV - \int_{A_s} S_i \delta x_i dA \tag{6}$$

must vanish at all points along the path of the motion for all virtual displacements (δx_i) satisfying the displacement boundary conditions. The virtual displacements can be expressed in terms of the virtual displacements of the nodes as

$$\delta x_i = \sum_{j=1}^{N_p} \delta x_{ij} \Phi_j \tag{7}$$

If the virtual displacement components of the kth node are in turn set equal to unity while all other nodal virtual displacement components are set equal to zero, the following equations of motion result

$$\sum_{j=1}^{N_p} \ddot{x}_{ij} \int_V \rho \Phi_j \Phi_k dV = -\int_V \sigma_{im} \frac{\partial \Phi_k}{\partial x_m} dV + \int_{A_s} S_i \Phi_k dA \tag{8}$$

At this point two approximations are introduced to make the equations of motion more manageable.

First, constant stress is assumed within each element. This approximation greatly reduces the amount of storage and computational time required for solution; however, it can lead to the presence of "keystoning" or "zero-energy" deformation modes. These can be suppressed by the introduction of a suitable viscosity.

Second, an approximate diagonal mass matrix is formed by lumping the off-diagonal terms on the left-hand-side of Equations 8, that is, the mass at the kth node is taken as

$$m_k = \sum_{j=1}^{N_p} \int_V \rho \Phi_j \Phi_k dV = \int_V \rho \Phi_k dV \tag{9}$$

where the second equality can be proved by integrating over individual elements, expressing the basis functions in terms of the shape functions and using the identity $\sum_{j=1}^{8} \Phi_j = 1$.

With these approximations, Equations 8 become

$$m_k \ddot{x}_{ik} = -\sum_{j=1}^{N_e} \left[\sigma_{im} \int_{V_j} \frac{\partial \Phi_k}{\partial x_m} dV \right] + \int_{A_s} S_i \Phi_k dA \quad \text{(k not summed)} \tag{10}$$

where N_e is the number of elements and the subscript j refers to the jth element.

TIME INTEGRATION SCHEME

Equations 10 are integrated approximately using an explicit central difference scheme. It is assumed that the nodal coordinates (x_{ik}^n) at time t^n are known, and that the nodal velocity components ($\dot{x}_{ik}^{n-1/2}$) during the previous time step $\Delta t^{n-1/2}$ are also known. The nodal acceleration components are calculated using Equations 10. These components are assumed constant over the new time step $\Delta t^{n+1/2}$, and the nodal velocity components are updated using

$$\dot{x}_{ik}^{n-1/2} = \dot{x}_{ik}^{n-1/2} + \ddot{x}_{ik}^{n} \frac{(\Delta t^{n-1/2} + \Delta t^{n+1/2})}{2} \tag{11}$$

Similarly, the nodal coordinates are updated by

$$x_{ik}^{n+1} = x_{ik}^{n} + \dot{x}_{ik}^{n+1/2} \Delta t^{n+1/2} \tag{12}$$

Once the velocities and positions of nodal points have been updated, the strain rate (more properly the deformation rate) at the center of each element can be determined and used to update the element stresses through the constitutive relations. Then the procedure can be repeated for the next time step.

To damp out localized oscillations of the concentrated masses associated with the passage of shock waves through the material, an artificial viscosity pressure is introduced in the form

$$p = \begin{cases} C_1 \rho \ell_{min} c |d_v| + C_2 \rho \ell_{min}^2 d_v^2, \text{ if } d_v < 0 \\ 0, \text{ if } d_v \geq 0 \end{cases} \tag{13}$$

where

C_1, C_2 = constants
ℓ_{min} = minimum of element edge and diagonal lengths
c = uniaxial sound speed in element
d_v = d_{ii}, the volumetric deformation rate where the deformation rate components (d_{ij}) will be defined in Equations 18.

The quadratic term is intended to damp out gradients associated with shock waves, the linear term is added to eliminate additional spurious oscillations. This artificial viscosity pressure is added to the normal stress components (σ_{11}, σ_{22}, σ_{33}) calculated from the material constitutive relations before introduction into Equations 10.

This integration scheme is only conditionally stable. To ensure stability the time step must be kept below a critical value dependent on the material sound speed and the element dimensions. A critical time step for each element is computed at each time step using the formula

$$\Delta t_{crit} = \frac{\ell_{min}}{C_1 c + C_2 \ell_{min} |d_v| + \sqrt{(C_1 c + C_2 \ell_{min} |d_v|)^2 + c^2}} \tag{14}$$

which accounts for artificial viscosity effects. The time step used for the next integration step is taken as 0.9 times the minimum of the critical time step values for all the elements.

EVALUATION OF INTEGRALS

The volume integrals in Equations 10 are evaluated approximately within each element by 8-point Gaussian quadrature. Thus

$$\int_{V_j} \chi dV = \int_{-1}^{1}\int_{-1}^{1}\int_{-1}^{1} \chi |J| da_1 da_2 da_3 \cong \sum_{k=1}^{8} \chi_k |J|_k \tag{15}$$

where

χ = an arbitrary integrand

$|J| = e_{ijk} \frac{\partial x_i}{\partial a_1} \frac{\partial x_j}{\partial a_2} \frac{\partial x_k}{\partial a_3}$, the Jacobian determinant of the transformation of Equations 4

k = subscript indicating that the subscripted quantities are to be evaluated at the Gaussian quadrature points, $a_i = \pm 1/\sqrt{3}$

The area integrals in Equations 10 are evaluated similarly using 4-point Gaussian integration.

Partial derivatives of the basis functions (shape functions) with respect to the global coordinates are evaluated using an appropriate chain rule. Thus,

$$\frac{\partial \Phi_j}{\partial a_i} = \frac{\partial \Phi_j}{\partial x_k} \frac{\partial x_k}{\partial a_i} \tag{16}$$

Equations 16 can be solved simultaneously to yield the partial derivatives.

$$\frac{\partial \Phi_j}{\partial x_i} = \frac{1/2 e_{imn} e_{rst} \frac{\partial \Phi_j}{\partial a_r} \frac{\partial x_m}{\partial a_s} \frac{\partial x_n}{\partial a_t}}{|J|} \tag{17}$$

Expressions for the partial derivatives with respect to the local coordinates appearing in the right-hand-sides of Equations 17 are obtained by differentiating Equations 3 and 4.

CONSTITUTIVE RELATIONS

A finite strain elastic-plastic material representation with von Mises yielding and a linear combination of isotropic and kinematic hardening as described by Key and Krieg is used.[2,3] The deformation rate components are

$$d_{ij} = \frac{1}{2}\left(\frac{\partial \dot{x}_i}{\partial x_j} + \frac{\partial \dot{x}_j}{\partial x_i}\right) \tag{18}$$

The normal deformation rate components are the material stretchings and the mixed components are the shearings. The spin components are

$$w_{ij} = \frac{1}{2}\left(\frac{\partial \dot{x}_i}{\partial x_j} - \frac{\partial \dot{x}_j}{\partial x_i}\right) \tag{19}$$

When the material is behaving elastically, the stress rate components are given in terms of the strain rate and spin components by

$$\dot{\sigma}_{ij} = 2\mu d_{ij} + \lambda \delta_{ij} d_{kk} + w_{ik}\sigma_{kj} + w_{jk}\sigma_{ki} \tag{20}$$

where λ and μ are the Lame constants. The first two terms on the right-hand-sides of Equations 20 are the contributions due to material straining, while the third and fourth terms are due to material rotation.

A von Mises yield function is defined as

$$\phi = |\xi|^2 - R^2 \begin{cases} < 0 \text{ for elastic behavior} \\ = 0 \text{ for plastic behavior} \end{cases} \tag{21}$$

[3] Sandia Laboratories. *An Efficient Numerical Method for Time Independent Plasticity*, by R. D. Krieg. Albuquerque, N. Mex., November 1977. (SAND77-0943, publication UNCLASSIFIED.)

where R is the radius of the yield surface in stress space and $|\xi|$ is an effective stress defined as

$$|\xi| = \sqrt{\frac{3}{2}\,\xi_{ij}\xi_{ij}} \tag{22}$$

where the quantities ξ_{ij} are the deviatoric parts of the differences between the stress components and the coordinates, α_{ij}, of the center of the yield surface in stress space; i.e., $\xi_{ij} = \sigma_{ij} - \alpha_{ij} - \frac{1}{3}\delta_{ij}(\sigma_{kk} - \alpha_{kk})$.

The radius of the yield surface and the time derivatives of the coordinates of its center are given by

$$R = Y_o + \beta H \bar{\epsilon}_p$$

$$\dot{\alpha}_{ij} = (1 - \beta)H\dot{\bar{\epsilon}}_p \frac{(\sigma_{ij} - \alpha_{ij})}{|\xi|} + w_{ik}\alpha_{kj} + w_{jk}\alpha_{ki} \tag{23}$$

where

Y_o = initial yield stress in a uniaxial test
E = elastic modulus from a uniaxial test
$H = EE_p/(E - E_p)$; E_p = plastic modulus from a unixial test
β = parameter in the range $0 \leqslant \beta < 1$ to control the hardening behavior; if $\beta = 0$ the behavior is kinematic, if $\beta = 1$ the behavior is isotropic.

The effective plastic strain rate $\dot{\bar{\epsilon}}_p$ and the effective plastic strain $\bar{\epsilon}_p$ are defined as

$$\dot{\bar{\epsilon}}_p = \sqrt{\frac{2}{3}\,d^p_{ij}d^p_{ij}}$$

$$\bar{\epsilon}_p = \int_o^t \dot{\bar{\epsilon}}_p dt \tag{24}$$

(The superscript p denotes the plastic part of the deformation rate.)

In the time integration scheme a trial stress is calculated at each time step assuming elastic behavior. Thus, using Equations 20

$$\sigma^T_{ij} = \sigma^n_{ij} + \dot{\sigma}^{n+1/2}_{ij}\Delta t^{n+1/2} \tag{25}$$

where the superscript T denotes the trial state.

The trial stress is substituted into Equation 21 to calculate a trial value of the yield function. If $\phi^T \leq 0$ then the process is elastic and the final stress state is the trial stress state. If $\phi^T > 0$ then the process is at least partly plastic and further calculation must be made.

The increment of effective plastic strain over the time step and the value of the effective plastic strain at the end of the time step are[3]

$$\Delta\bar{\epsilon}_p^{n+1/2} = \frac{1}{3G}\frac{|\xi|^T - R^n}{1 + H/3G}$$

$$\bar{\epsilon}_p^{n+1} = \bar{\epsilon}_p^n + \Delta\bar{\epsilon}_p^{n+1/2} \tag{26}$$

The trial stress components are scaled back to the yield surface by

$$\sigma_{ij}^{n+1} = \sigma_{ij}^T - c_\sigma \xi_{ij}^T \tag{27}$$

where

$$c_\sigma = \frac{1}{1 + H/3G}\frac{|\xi|^T - R^n}{|\xi|^T}$$

The new coordinates of the center of the yield surface are

$$\alpha_{ij}^{n+1} = \alpha_{ij}^n + \dot{\alpha}_{ij}^{n+1/2}\Delta t^{n+1/2} \tag{28}$$

where the time derivatives are obtained from Equations 23 with $\dot{\bar{\epsilon}}_p = \Delta\bar{\epsilon}_p^{n+1/2}/\Delta t^{n+1/2}$.

CIRCUMFERENTIAL SEGMENTATION REDUCTION

Examination of Figure 2 reveals that the method used to divide the body into elements can result in a large concentration of elements near the Z-axis. In most instances, the region of primary structural interest, and the region where most elements are desired, is the case wall near the outer radius. Fine detail near the centerline is superfluous and adds to the run time. Moreover, the small circumferential dimensions of elements near the axis can impose an undesirably small time step on the solution.

To alleviate this problem, a method for reducing the number of elements in the circumferential direction by one-half was devised. This is illustrated in Figure 4, where the shaded area represents the region of coarser segmentation. At the transition

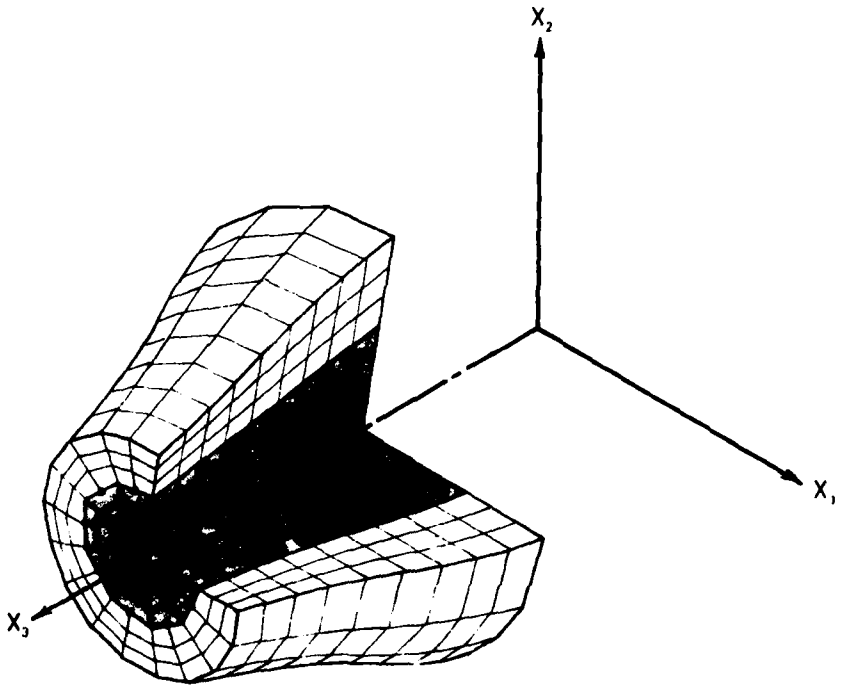

FIGURE 4. Finite Element Model with Circumferential Segmentation Reduction.

from finer to coarser segmentation, nodal points not forming a corner of one of the coarser elements are constrained to always remain midway between the nodes on either side. The constrained nodal points are indicated by black dots in the figure. The masses of the constrained nodal points are lumped equally at the nodes on either side. Satisfaction of the virtual displacement equations requires that the nodal forces on the constrained nodal points also be divided equally between the nodes on either side.

This technique can result in a substantial computational savings through a reduction in the concentration of elements near the centerline. It can also be used to provide a less detailed representation of the explosive filler, which can often be tolerated when the structural integrity of the case is of primary concern in the analysis. The suddenness of the reduction of one-half in radial segmentation is mitigated by the shrinking of the circumferential dimensions of the elements with decreasing radius so that in practice a reasonably uniform grid can be obtained. More than one level of segmentation reduction can be used if desired.

COMPUTER IMPLEMENTATION

THE WHAP CODE

A computer code called WHAP (Warhead Analysis Program) has been written implementing the theory described in the previous section. During problem solution a large amount of nodal and element data must be stored and assessed. It is not possible to fit a reasonable-sized problem into the standard 65K address space of the UNIVAC 1100/82 computer. Two versions of the code were written to attempt to deal with this difficulty.

In the initial version of the program nodal displacements, velocities and forces were stored sequentially by plane on tape (logical unit 13). Element stresses, effective plastic strains, and yield surface center coordinates were stored sequentially by segment on a second tape (logical unit 14). Only the nodal data for the ith and (i+1)th planes and the element data for the ith segment were stored in core memory at any one time. This scheme suffered from two drawbacks. First, a large amount of input/output time was required for reading and writing the tapes. Second, it was not feasible to take advantage of the segmentation reduction scheme described previously.

In the second version of the program, the "@FTN,O" compiler option was used to permit accessing addresses over 65K. Thus, the entire program and data were stored in extended memory removing the need for storage tapes. Although there is a penalty in terms of slower execution speed, the two drawbacks of the first version are eliminated. Only the second version will be described in this report.

FUNCTIONING OF WHAP CODE

An abbreviated flow diagram for the WHAP code is shown in Figure 5. As indicated in the figure the functioning of the program can be broken down into three phases: setup, solution, and end. These will be discussed in turn.

Setup operations are performed first. The start tape for the problem and a solution and output times card are read. Based on nodal point cylindrical coordinates in the generating plane, the rectangular cartesian coordinates of all nodal points are determined. Nodal forces due to element surface pressures at the solution start are calculated. It is assumed that the applied loading, although non-axisymmetric, has a plane of symmetry such that only half the warhead (from $\theta = 0$ to $\theta = \pi$) need be analyzed. The mass matrix is calculated and an initial time step determined. Other initializations as well as the printing of heading information and solution and output times data are also carried out.

In the solution phase, the approximate time integration of the equations of motion is performed. At each time step the nodal velocities and positions are updated

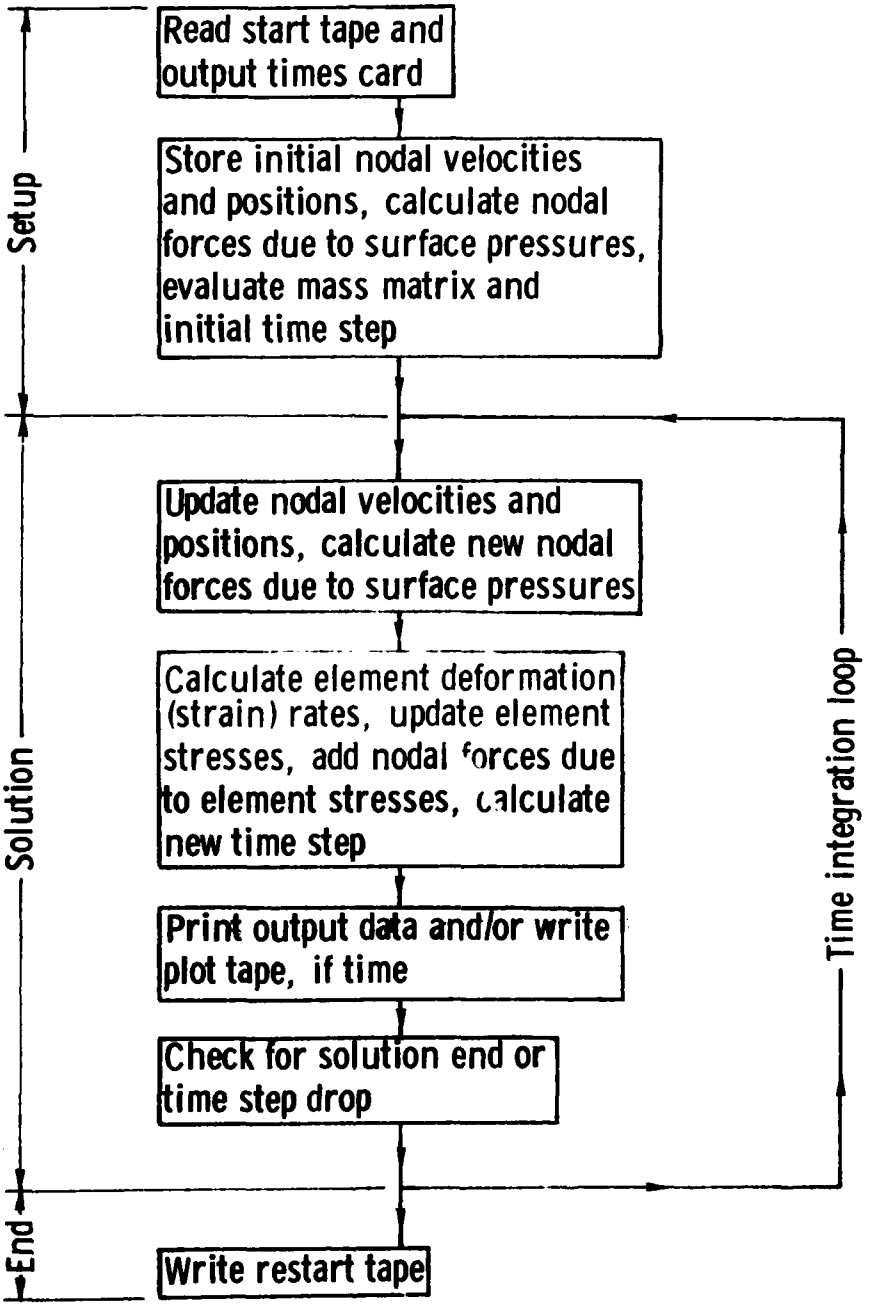

FIGURE 5. Flow Diagram of WHAP Code.

using the central difference formulas, and new nodal force contributions due to element surface pressures are calculated. Based on the new nodal velocities and positions, element deformation rates and spins can be determined. These are used to update the element stresses through the constitutive relations. Nodal force contributions due to element stresses are calculated and added to the forces due to surface pressures. With the integration step essentially complete, an output data print and/or plot tape writes can be made if called for by the output times card. Finally, checks are made to see if the end of the solution time period has been reached or if an excessive time step drop has occurred indicating that the solution should be terminated. If not, the integration procedure is repeated.

At the end of the run a restart tape having the same format as the original start tape is written (except that additional nodal and element data are included). Problem solution can be continued using this tape and a new solution output times card. This feature permits checking to see how a problem is progressing before too much computer time has been wasted on an unsatisfactory solution.

OVERALL PROBLEM SOLUTION

The overall problem solution procedure including the pre- and post-processing required for use of the WHAP code is indicated in the flow diagram in Figure 6. A two-dimensional quadrilateral mesh for the generating plane is created interactively on the HP9845A Desktop Computer using program MESH. Interactive input of other required data is accomplished using program INWHAP. These mesh and input data are transmitted in the form of card images to the UNIVAC 1100/82 computer and stored in a file using the HP9845A as a remote terminal. Program WHAPST is then executed on the UNIVAC 1100/82 to transform the file data into a start tape for the WHAP program. A small amount of additional data (regarding solution and output times) is input during running of the WHAP code itself, which performs the approximate time integration. Printed output and plot tapes are generated during execution. Post-processing programs DFSTRW and CNTRW are used to obtain deformed structure and stress contour plots from the plot tapes. Additional plot specification cards are required for the running of these programs.

USER INFORMATION

For reference purposes, a list of most of the variables used in the WHAP code is given in Appendix A. Brief descriptions of the subroutines making up the code are given in Appendix B. User instructions for the WHAP code and associated pre- and post-processors are given in Appendix C.

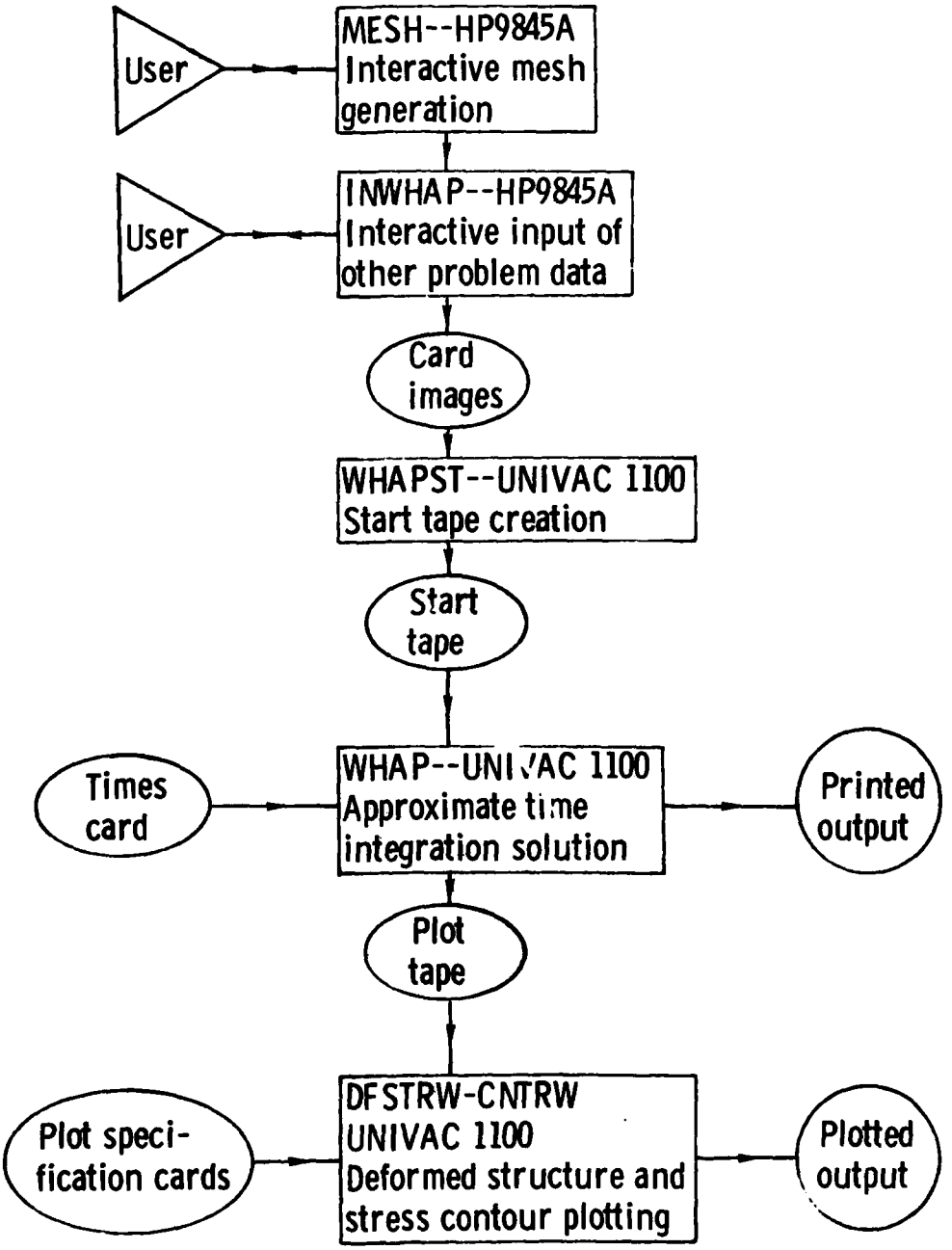

FIGURE 6. Flow Diagram of Overall Problem Solution.

CODE CHECKOUT

Checkout of a computer code such as this can be accomplished in two main ways:

1. By using the code to solve a problem for which an analytic solution exists
2. By comparing the code results with results of another, already-verified code for the same problem.

The first of these methods is doubtless the more elegant. However, in the case of bodies subjected to non-axisymmetric impulsive loadings, suitable analytic solutions are not available. Hence, the second method was used (although an attempt was made to indicate that the results are reasonable in the light of elementary theory). The HONDO II code was used for comparison purposes. Two checkout problems were run.

Checkout Problem No. 1

The first checkout problem involved an elastic-plastic rod subjected to a step pressure loading at one end. The rather coarse finite element grid used for both the WHAP and HONDO II runs is shown in Figure 7. The geometric and material parameters defining the problem are also indicated. Eight circumferential segments were used in the WHAP code model.

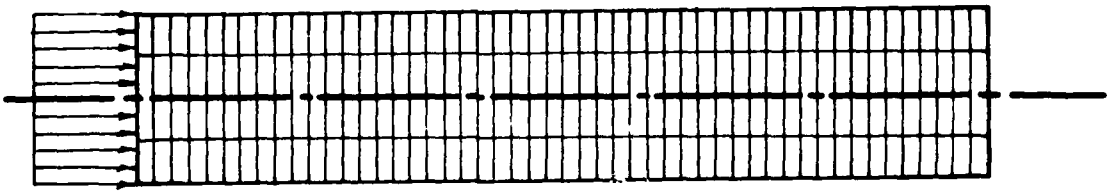

$L/D = 5$

$E/E_p = 4$

$\nu = .3$

$p/Y = 2$

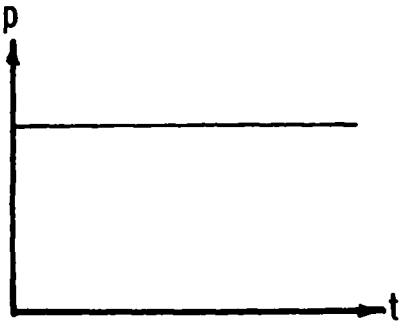

FIGURE 7. Elastic-Plastic Rod Subjected to Step Pressure at One End.

Axial stress versus distance from the impacted end of the rod is plotted in Figure 8. The HONDO II and WHAP results are quite close to one another. The use of more segments would probably have produced even better agreement. The dashed line in the figure is the result obtained from one-dimensional rod theory. Differences between the finite element and theoretical results are due primarily to transverse inertia effects. A rod with a higher length-to-diameter ratio might have yielded results more nearly in accord with one-dimensional theory. However, errors in the code associated with transverse effects might not have been apparent in such a model.

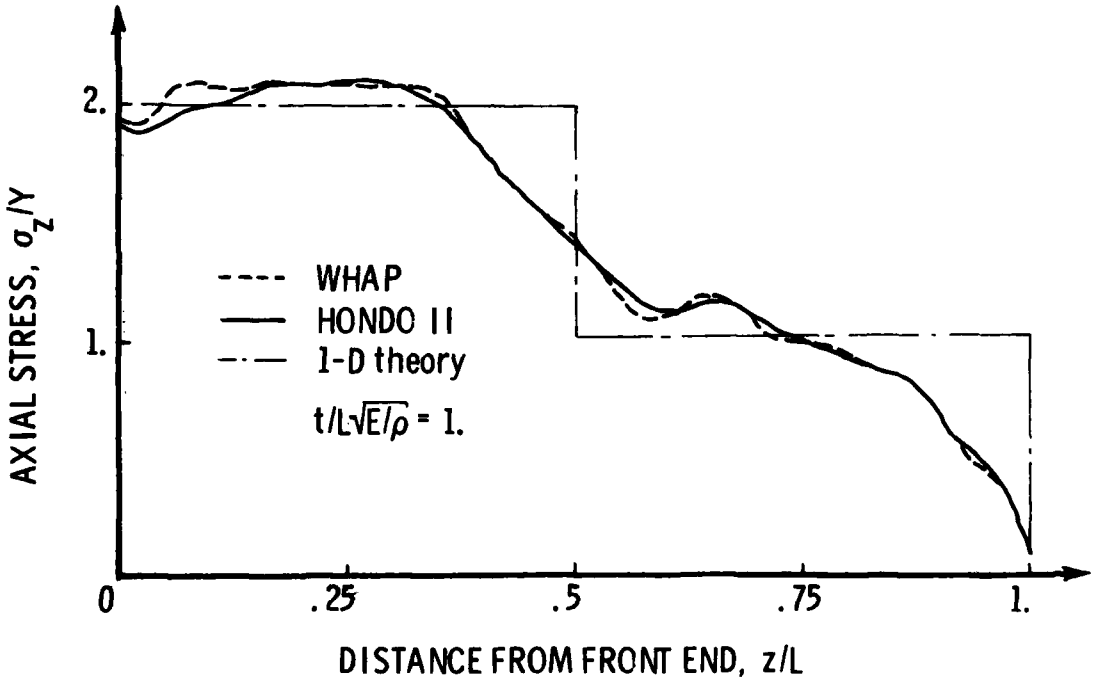

FIGURE 8. Axial Stress Versus Distance From Front End for Elastic-Plastic Rod Subjected to Step Pressure.

Checkout Problem No. 2

The loading in the first checkout problem was axisymmetric. Hence, this first problem did not test the non-axisymmetric part of the coding. The second checkout problem involved an elastic ring subjected to a ramp pressure on its outer surface that varied sinusoidally around the circumference of the ring. Plane strain was assumed. The HONDO II code has the capability of solving such a plane strain problem. (A large constant value is added to all the nodal radii in the model.) A WHAP code solution was obtained treating the ring as a solid of revolution subjected to a non-axisymmetric loading. The finite element models used and the parameters defining the

problem are given in Figure 9. One hundred circumferential segments were used in the WHAP model, which is the same as the number of quadrilaterals around the circumference of the HONDO II model.

Stress parallel to the surface in the first layer of elements beneath the load is plotted versus circumferential angle in Figure 10. The slight difference between the WHAP and HONDO II results may be due to a difference in the way the artificial viscosity is calculated in the two codes. In an axisymmetric elastic body subjected to sinusoidal loading one would expect sinusoidal variation in the stress as well. Except for the slight bump at low angles, the curves are nearly sinusoidal. (A sine curve with the same maximum amplitude could have been superposed on the finite element results but was omitted for clarity.)

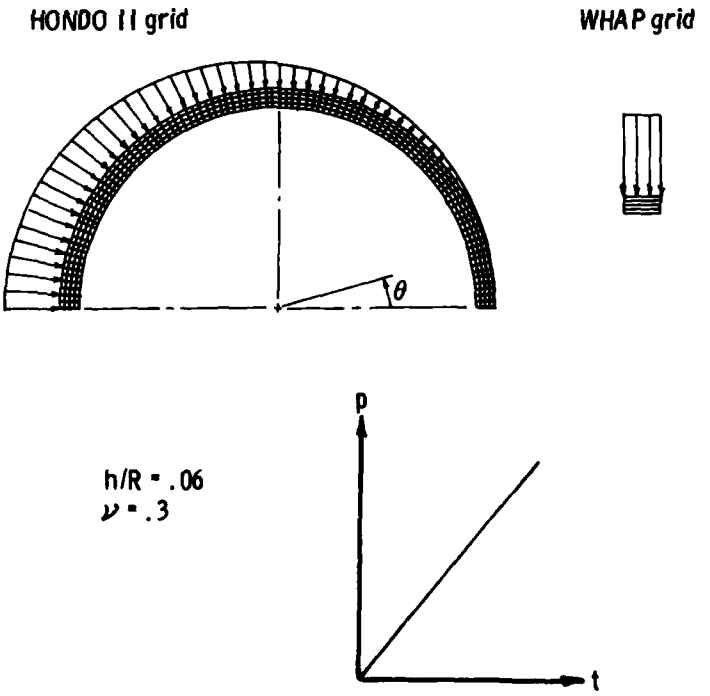

FIGURE 9. Elastic Ring Subjected to Ramp Pressure Sinusoidally Varying Around Circumference.

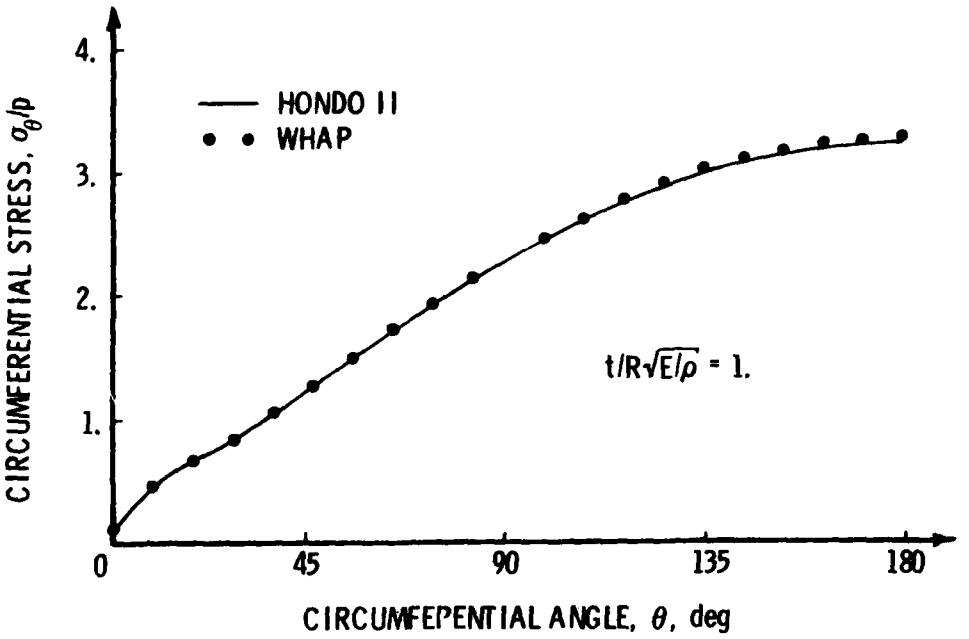

FIGURE 10. Circumferential Stress vs. Angle for Elastic Ring Subjected to Ramp Pressure.

ANALYSIS OF PROJECTILE IMPACTING SIMULATED CONCRETE

SMALL PROJECTILE FIRINGS

Experimental firings of small steel projectiles at normal incidence against simulated concrete half-space and thin steel plate targets are described by Stronge and Schulz.[4] The uninstrumented test projectiles were flat-fronted cylinders with an internal cavity and were intended to roughly represent warheads. During penetration the projectiles developed a bulge near the front of the internal cavity and, at high enough impact velocities, fractured in this region. Projectile deformations measured after testing were compared with finite element analysis results obtained using the HONDO II code.

Similar firings of projectiles against targets at obliquity are described by Schulz and Heimdahl.[5] Some of the projectiles tested at obliquity were filled with an explosive simulant (plaster of Paris) while others were left unfilled. A cross-sectional view of

[4] W. J. Stronge and J. C. Schulz. "Projectile Impact Damage Analysis," in *Papers Presented at the Symposium on Computational Methods in Non-linear Structural and Solid Mechanics*, edited by Ahmed K. Noor and Harvey G. McComb, Jr. Pergamon Press, New York, 1981. (Also published as special issue of *Journal of Computers and Structures*, Vol. 13, No. 1-2 (2981). pp. 287-294.)

[5] Naval Weapons Center. *Oblique Impact Projectile Damage*, by J. C. Schulz and O. E. R. Heimdahl. China Lake, Calif., NWC, January 1982. (NWC TM 4695, publication UNCLASSIFIED.)

the projectile used in oblique impact firings is shown in Figure 11. In addition to bulging, projectiles fired at obliquity also bent such that the centerline of the nose and case portions were not colinear.

Measurements of the final deformed shapes of projectiles from these oblique impact firings were compared with WHAP code analytical results. Such a comparison does not provide an especially critical test of code performance. Even when reasonable agreement is obtained, stress values may differ considerably between analysis and experiment. However, since projectile stresses were not measured (due to the difficulties in providing suitable instrumentation), no other comparison appeared feasible.

PROJECTILE ANALYSIS TECHNIQUE

A structural analysis technique for projectiles impacting hard targets at normal incidence has been developed at the Naval Weapons Center.[1,4] This technique involves finding an approximate loading history to be applied to the front of the projectile to represent forces at the target-projectile interface and then using this approximate loading in a nonlinear finite element analysis to calculate stresses and deformations in the projectile. This same technique can be used for projectiles impacting at obliquity if the loading history is modified to account for non-axisymmetric effects.

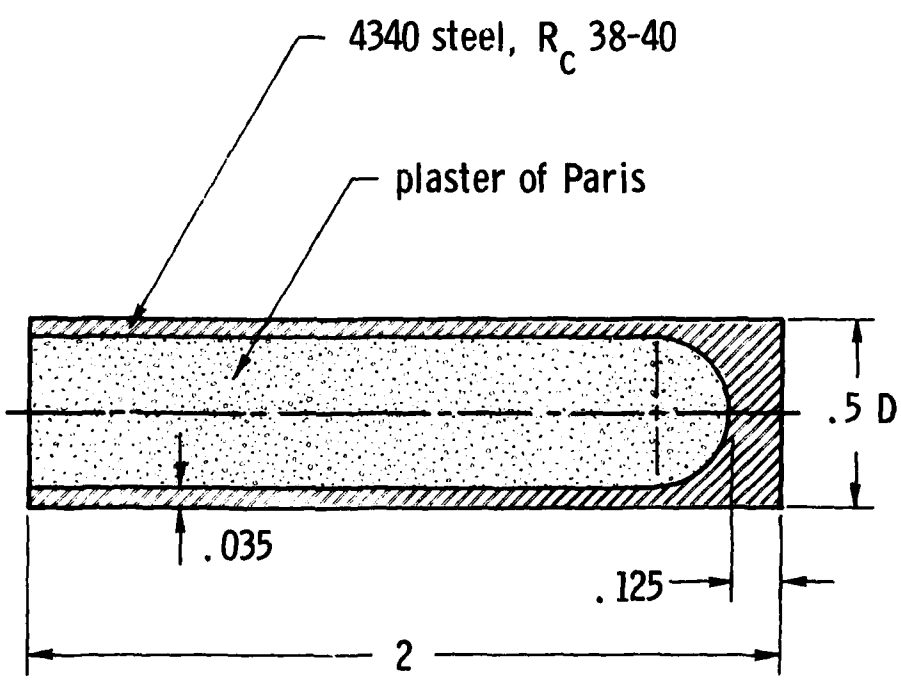

FIGURE 11. Cross-Sectional View of Projectile Used for Oblique Firings.

PROJECTILE SELECTED FOR ANALYSIS

To keep run costs down, an unfilled projectile (without the plaster of Paris) was considered for analysis. The impact velocity of the projectile was taken as 2,155 ft/s (corresponding to one of the unfilled test projectiles fired at normal incidence). WHAP code runs were made using loading histories corresponding to penetration into a concrete half-space at normal incidence and at 45 degrees obliquity. For comparison purposes, a HONDO II run at normal incidence was also made. The solution was stopped at a maximum of 75 microseconds by which time plastic deformation of the projectile appeared to have ceased.

FINITE ELEMENT MODEL

A model of the projectile containing 264 nodal points and 198 elements in the generating plane was constructed. Ten radial planes were used to divide the projectile into nine segments circumferentially. The 4340 steel was modeled as an elastic, perfectly plastic material with the properties given in Table 1.

TABLE 1. Material Properties for 4340 Steel.

Young's modulus, psi	30,000,000
Poisson's ratio	0.3
Dynamic yield stress, psi	177,000
Density, lb sec^2/in^4	0.000733

LOADING HISTORIES

For impact at normal incidence a loading history was obtained using the method of Stronge and Schulz.[4] This loading history consisted of a quasi-steady-state penetration theory drag force[6] to which was added an initial transient to account for start-up conditions. The force was applied as a pressure uniformly distributed over the front end of the projectile. For impact at obliquity two different loading histories were used.

In the first loading (Load No. 1), the same pressure as a function of time was used as for normal impact, except that the application time was shifted. Initially, pressure was applied only at the leading edge of the projectile (the edge that impacted the target first). As the projectile moved forward and more of its front end crossed the plane of the target the pressure was applied over this portion of the front end as

[6] Defense Nuclear Agency. *Projectile Penetration in Earth Materials: Theory and Computer Analysis*, by R. S. Bernard and D. C. Creighton. Washington, D.C., November 1977. (Contract Report S-76-13, publication UNCLASSIFIED.)

well. Only when the projectile was completely imbedded was pressure applied over the entire front end. The effect was a pressure that swept across the front surface of the projectile as this surface reached the target.

This loading did not produce results in agreement with experiment. Consequently, a second loading (Load No. 2) was used. In this second loading, the magnitude of the pressure at the leading edge was increased by 5% and the magnitude of the pressure at the trailing edge was decreased by 5%. The pressure was allowed to vary linearly across the front surface between these extremes. Some rationale for this second loading will be given later.

FINITE ELEMENT RESULTS

The WHAP code results for the final deformed shapes of projectiles impacting simulated concrete at normal incidence and at 45 degrees obliquity (Load No. 2) are shown in Figure 12. Qualitatively, the analytically determined shapes agree well with

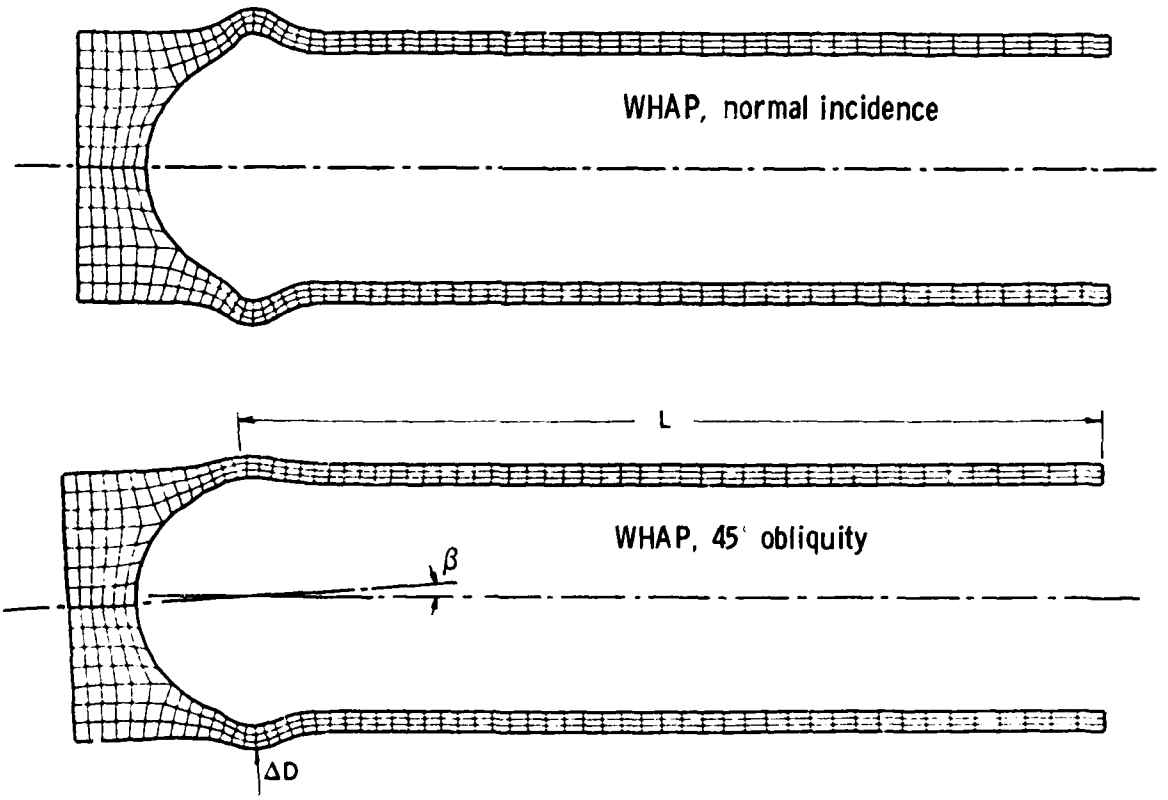

FIGURE 12. Final Deformed Shapes of WHAP Models of Projectiles Impacting Simulated Concrete at 2,155 ft/s at Normal Incidence and 45 Degrees Obliquity.

the shapes of test projectiles illustrated photographically by Schulz and Heimdahl.[5] To obtain a quantitative comparison, the increase in diameter at the bulge, the angle between nose and case centerlines and the distance from the bulge to the rear of the projectile (D, θ, and L in the figure) were measured for the test projectiles. A tabulation of measured and analytically determined values is given in Table 2. (No firing was made at 2,155 ft/s and 45 degrees obliquity so data at 2,200 and 2,240 ft/s were extrapolated for the table.)

TABLE 2. Comparison of Analytical and Test Results for Small Projectile Impacting Simulated Concrete at 2,155 ft/s.

	Normal incidence			45 degrees obliquity		
	HONDO II	WHAP	Test projectile	WHAP Load no. 1	WHAP Load no. 2	Test projectile
Increase in diameter at bulge, ΔD, in.	0.088	0.090	0.084	0.046	0.047	0.052
Angle between nose and case centerlines, β, deg.	...	...	...	0.9	3.7	4.4
Distance from bulge to rear of projectile, L, in.	1.60	1.59	1.60	1.59	1.59	1.60

For impact at normal incidence there is good agreement between the predictions of the HONDO II and WHAP codes and the measured values. For impact at 45 degrees obliquity, the diameter increases and the distances from the bulge to the rear of the projectiles predicted by the WHAP code with the two different loadings are in good agreement with each other and also with the experimental results. However, the bend angle predicted with Load No. 1 is considerably less than that predicted with Load No. 2, which agrees fairly well with experiment. An explanation for this behavior is as follows: Compared to impact at normal incidence, there is extra target material on the leading edge side of the projectile. This extra material can be expected to produce some additional confinement and an increase in the pressure loading on this side. Conversely, there is a lack of material on the trailing edge side of the projectile, which can be expected to reduce the pressure loading. The ±5% adjustment that was made to the loading magnitude has no especial justification except that it produced better results.

RUN COSTS

Oblique impact runs for this problem using the WHAP code proved to be quite expensive. Run costs on the Naval Weapons Center UNIVAC 1100/82 were approximately $2,700 versus $140 for comparable WHAP and HONDO II runs. CPU times per time step were 6.67 versus 0.34 with the two programs.

CONCLUSION

A program for the structural analysis of axisymmetric warheads impacting targets at obliquity has been developed. The WHAP code itself, as well as pre- and post-processors required for complete problem solution, have been written and checked out, and the entire package is now operational. Results obtained for the analysis of a small steel projectile penetrating into a simulated concrete half-space at both normal incidence and 45 degrees obliquity appear reasonable.

One objective of this work was to produce a code that is inexpensive to use. This goal was not attained. Run costs using the WHAP code are an order of magnitude higher than for the two-dimensional code, HONDO II. As a result, analyses of warheads impacting at obliquity using the new code will probably not be performed as routinely as analyses of warheads impacting at normal incidence. However, the code is available for situations where the effects of obliquity are of especial interest--and where money is available for making runs.

The small projectile problem that was run points out the need for better characterization of the loading histories of projectiles impacting targets at obliquity. Reasonable agreement between code and test results was obtained only by artificially adjusting the loading used. Almost no data regarding the effects of obliquity on penetration forces are available, especially for the initial transient stage of loading behavior. Work needs to be done in this area to provide input for running of the WHAP code.

Appendix A
DEFINITIONS OF VARIABLES

Definitions of most of the variables used in the WHAP program are listed for reference in this appendix.

COMMON/ZVAR/variables

- Z(NDIMZ), main storage array for program
- IZ(NDIMZ), integer equivalent of Z array
- NDIMZ, maximum dimension of Z array
- N2–N22, integers giving starting locations for program variables stored in Z array

COMMON/BK1/variables

- NNP, number of nodal points in generating plane
- NEL, number of quadrilateral element traces in generating plane
- MPLN, maximum number of radial planes in circumferential direction (in regions of finest circumferential segmentation)
- MSEG, maximum number of elements in circumferential direction = MPLN - 1
- MNP, total number of nodal points
- MEL, total number of elements
- NCNP, number of circumferential arcs with constrained nodal points (for transition to coarser circumferential segmentation)
- NMAT, number of materials
- NESP, number of element surface pressures
- NLTC, number of load-time curves
- MLP, maximum number of load points on any load-time curve
- HED(20), problem title
- IDT, date initial start tape created
- ITM, time of day initial start tape created
- NSTRT, start number
- VZ0, initial axial velocity

COMMON/BK2/variables

- A(8), values of local a-coordinate at Gaussian quadrature points
- B(8), values of local b-coordinate at Gaussian quadrature points
- C(8), values of local c-coordinate at Gaussian quadrature points
- P(4,4), shape function values at Gaussian quadrature points in element surface used in calculation of loads due to surface pressures
- PP(8,8), shape function values at Gaussian quadrature points inside element
- DPDA(8,8), derivatives of shape functions with respect to a-coordinate at Gaussian quadrature points
- DPDB(8,8), derivatives of shape functions with respect to b-coordinate at Gaussian quadrature points
- DPDC(8,8), derivatives of shape functions with respect to c-coordinate at Gaussian quadrature points
- THSEG, π/MSEG, angle between planes corresponding to finest segmentation

COMMON/BK3/variables

TT, current time in solution integration
DT1, old time step
DT2, new time step
DTO, initial time step x 10-5, used to check for time step drop
DTN, time step in a given element, used in determining new time step
NELCRT, element with critical time step
NSGCRT, segment containing element with critical time step
NSTEP, number of current integration step
B1, coefficient of quadratic term in artificial viscosity
B2, coefficient of linear term in artificial viscosity
B3, coefficient in keystone viscosity

COMMON/BK4/variables

TPRT1, initial time for printed output
TPRT2, final time for printed output, solution end
DTPRT, time interval for printed output
TPLT1, initial time for plotted output
TPLT2, final time for plotted output
DTPLT, time interval for plotted output
NDOUT(50), nodes at which displacement quantities are to be output
NLOUT(50), elements in which stresses are to be output
NPLOUT(20), planes for which displacement quantities are to be output
NSGOUT(20), segments for which stresses are to be output

COMMON/BK5/variables

DF, determinant of deformation gradient
D(6), deformation (strain) rate
W(3) spin (non-zero components)

Quantities stored unchanged in Z array throughout solution

Z(1)~R(NNP), radial coordinates of nodes in undeformed body
Z(N2)~Z(NNP), axial coordinates of nodes in undeformed body
IZ(N3)~BC(NNP), nodal boundary condition codes
IZ(N4)~NPLN(NNP), number of radial planes associated with nodal points in generating plane
IZ(N5)~ND(NNP), global nodal numbers cooresponding to generating plane nodal numbers
IZ(N6)~NDA(NNP), constrained node indicator for use in displacement update
IZ(N7)~NDC(NCNP), nodal numbers associated with circumferential arcs containing constrained nodes
IZ(N8)~NSEG(NEL), number of segments associated with element traces in generating plane
IZ(N9)~NL(NEL), global element numbers corresponding to generating plane element numbers
IZ(N10)~IX(5,NEL), element nodal point and material specifications

Z(N11)~PROP(15,NMAT), material properties
IZ(N12)~ISP(5,NESP), nodal points and load-time curves for pressurized surfaces
Z(N13)~PM(4,NESP), pressure multipliers at nodes on pressurized surfaces
Z(N14)~AT(NESP), arrival times for surface pressures
Z(N15)~LT(2,NLTC,MLP), load-time points
Z(N16)~MS(NNP), nodal masses
Z(N17)~DJ0(NEL), initial Jacobian determinants at element centers

Nodal quantities updated in Z array throughout solution
Z(N18)~XX(3,MNP), coordinates of nodal points in deformed body
Z(N19)~VV(3,MNP), velocity components of nodal points in deformed body
Z(N20)~FF(3,MNP), force components at nodal points in deformed body

Stress quantities updated in Z array throughout solution
Z(N21)~S(6,MEL), element stress components
Z(N22)~STRG(6,MEL), storage for element yield surface centers, effective plastic strains and state variables

Material properties (1–6 are input, 7–15 are calculated)
PROP(1,NMAT)~RO, density
PROP(2,NMAT)~E, Young's modulus
PROP(3,NMAT)~NU, Poisson's ratio
PROP(4,NMAT)~SY, uniaxial yield stress
PROP(5,NMAT)~ET, hardening modulus
PROP(6,NMAT)~BETA, hardening parameter
PROP(7,NMAT)~LMBDA=TWOG*NU/(1.–2.*NU)
PROP(8,NMAT)~TWOG=E/(1.+NU)
PROP(9,NMAT)~H=E*ET/(E–ET)
PROP(10,NMAT)~YR=.816496581*SY
PROP(11,NMAT)~CYR=.816496581*BETA*H
PROP(12,NMAT)~CEP=.816496581*TWOG
PROP(13,NMAT)~CCIG=1./(1.+H/1.5/TWOG)
PROP(14,NMAT)~CCA=H/1.5/TWOG*(1.–BETA)
PROP(15,NMAT)~CX=SQRT((LMBDA+TWOG)/RO)

Appendix B
SUBROUTINE DESCRIPTIONS

Brief descriptions of the subroutines making up the WHAP code are given in this appendix.

MAIN PROGRAM WHAP

This short routine acts as a driver for the remainder of the program. The size of the common variable Z, where most data is stored, can be changed by changing the parameter NDIMZ in this routine. WHAP calls subroutines SETUP and SOLVE.

SUBROUTINE SETUP (N2,N3,N4,N5,N6,N7,N8,N9,N10,N11,N12,N13,N14,
N15,N16,N17,N18,N19,N20,N21,N22,NDIMZ)

Reading of the start tape, and storage and initialization of problem variables are accomplished in this subroutine. SETUP calls subroutines LOAD, MASS, DETJ and STEP.

SUBROUTINE LOAD (ISP,PM,AT,LT,XX,FF,TT)

Nodal forces due to element surface pressure loads are calculated in this subroutine. Gaussian quadrature is used to evaluate the area integrals involved.

SUBROUTINE MASS (XX,ND,NDA,NSEG,IX,RO,MS)

Nodal masses are calculated in this subroutine. Gaussian quadrature is used to evaluate the volume integrals involved. An adjustment in the case of nodes at the transition from finer to coarser segmentation is performed.

SUBROUTINE DETJ (XX,IX,DJ)

The initial Jacobian determinant of the transformation of Equations 4 is calculated at the center of each element.

SUBROUTINE STEP (XX,IX,PROP)

An initial time step that ensures solution stability is calculated. At subsequent times this calculation is performed in subroutine FORCE.

SUBROUTINE SOLVE (R,Z,BC,NPLN,ND,NDA,NDC,NSEG,NL,IX,PROP,
ISP,PM,AT,LT,MS,DJ0,XX,VV,FF,S,STRG)

The approximate time integration solution is carried out in this subroutine. Nodal velocities and positions are updated and new nodal forces due to surface pressure loads are calculated. In a loop over the number of elements, element deformation rates and spins are calculated and used to update the element stresses. Contributions to the nodal forces due to element stresses are calculated and a new solution time step is determined. An output data print and plot tape writes are accomplished when requested. After the solution is completed a restart tape is written. SOLVE calls subroutines LOAD, STRAIN, STRESS and FORCE.

SUBROUTINE STRAIN (ND1,ND2,ND3,ND4,ND5,ND6,ND7,ND8,XX,VV,DJ0)

Calculation of the deformation rate and spin at the element center is accomplished in this subroutine. The deformation gradient at the element center is also determined.

SUBROUTINE STRESS (S,LMBDA,TWOG,YR,CYR,CEP,CCSIG,CCA,A,EP,STATE)

The constant element stress based on the deformation rate at the element center is calculated. An elastic trial stress is calculated and then scaled back to the yield radius if plastic flow has occurred.

SUBROUTINE FORCE (ND1,ND2,ND3,ND4,ND5,ND6,ND7,ND8,
RO,CX,XX,VV,FF,S,ISEG,NSEG)

Nodal forces due to the element stress are determined. Artificial and keystone viscosity contributions are included. An element time step is calculated.

Appendix C
USER INSTRUCTIONS

User instructions for the input of data to the pre-processor WHAPST, to the WHAP program itself, and to the post-processors DFSTRW and CNTRW are provided in this appendix.

A. Pre-processor WHAPST

This program generates a start tape (logical unit 8) for the WHAP code and also creates a plot of the undeformed generating plane. Input data for this program is usually created interactively on the HP9845A Desktop Computer and transmitted in the form of card images to the UNIVAC 1100/82. However, these card images could also be obtained by other means. The format for these card images is given below.

1. Heading card (20A4)
   Columns 1–80 HED(20), information to identify run

2. Mesh file card (A6)
   Columns 1–6 MF, name of mesh file on HP9845A (can be left blank if data not generated on HP9845A)

3. Storage file card (A6)
   Columns 1–6 SF, name of storage file on HP9845A (can be left blank)

4. Control card (10I5,E10.0)
   Columns 1–5 NNP, number of nodal points in generating plane
   Columns 6–10 NEL, number of elements in generating plane
   Columns 11–15 MPLN, maximum number of radial planes
   Columns 16–20 MSEG = MPLN–1
   Columns 21–25 NMAT, number of materials
   Columns 26–30 NESP, number of element surface pressures
   Columns 31–35 NLTC, number of load-time curves
   Columns 36–40 MLP, maximum number of points on any load-time curve
   Columns 41–45 NNC, number of nodal point specification cards
   Columns 46–50 NEC, number of element block specification cards
   Columns 51–60 VZ0, initial axial velocity

5. Nodal output cards (10I5, 5 cards)
   List of nodal points for which printed output is desired (50 points maximum, first zero or blank terminates list)

6. Element output cards (10I5, 5 cards)
   List of elements for which printed output is desired (50 elements maximum)

7. Radial plane output cards (10I5, 2 cards)
   List of radial planes for which printed output is desired (20 planes maximum)

8. Segment output cards (10I5, 2 cards)
   List of segments for which printed output is desired (20 segments maximum)

9. Nodal point specification cards (I5,2E10.0,I5,4X,I3,3X,2E10.0, NNC cards)

Columns 1–5	N, nodal point number
Columns 6–15	R(N), radial coordinate
Columns 16–25	Z(N), axial coordinate
Columns 26–30	INCR, nodal point generation increment, taken from last card read, BC of intermediate points is from previous card
Columns 35–37	BC(N), displacement boundary condition code
Columns 41–50	SR, spacing ratio for incremented points
Columns 51–60	RAD, radius of arc connecting end points along which points are generated

10. Element block specification cards (9I5, NEC cards)

Columns 1–5	MC1, nodal point number of one corner node of four-sided element block
Columns 6–10	MC2, nodal point number of second corner node of four-sided element block (progressing counter-clockwise)
Columns 11–15	MC3, nodal point number of third corner node
Columns 16–20	MC4, nodal point number of fourth corner node
Columns 21–25	MATL, material identification number
Columns 26–30	NLGRP, element group number for determining number of segments, if NLGRP = 0 then NLGRP = 1
Columns 31–35	NELRW, number of elements in row
Columns 36–40	NROWS, number of rows
Columns 41–45	NGEN, generation parameter, if NGEN = 0 nodal points in interior of block are found as intersections of straight lines connecting nodal points on corresponding sides, if NGEN > 0, interior nodal points are found using Laplace generation with NGEN iterations

11. Material specification cards (NMATL sets)
    a. Title card (20A4)

Columns 1–80	MTITLE, title to identify material

    b. Property card (6E10.0)

Columns 1–10	PROP(1), material density, RO
Columns 11–20	PROP(2), Young's modulus, E
Columns 21–30	PROP(3), Poisson's ratio, NU

Columns 31–40	PROP(4), yield stress, SY
Columns 41–50	PROP(5), hardening modulus, ET
Columns 51–60	PROP(6), hardening parameter, BETA

12. Element surface pressure specification cards (4I5, SE10.0, NESP cards)

Columns 1–5	ISP(1), first nodal point
Columns 6–10	ISP(2), second nodal point, two points must form one edge of element in generating plane
Columns 11–15	ISP(3), number of segment in circumferential direction
Columns 16–20	ISP(4), number of load-time curve
Columns 21–30	PM(1), pressure multiplier at first corner of surface element
Columns 31–40	PM(2), pressure multiplier at second corner
Columns 41–50	PM(3), pressure multiplier at third corner
Columns 51–60	PM(4), pressure multiplier at fourth corner
Columns 61–70	AT, arrival time of pressure at element surface

13. Load-time curve specification cards (NLTC sets)
    a. Load-time cards (2E10.0, MLP cards)

Columns 1–10	LT(1), time
Columns 11–20	LT(2), load

B. WHAP program

Most input data for this program is obtained from the start tape written by WHAPST (or from a restart tape written by WHAP itself). This start tape is read by WHAP on logical unit 8. Three blank tapes must be assigned for the writing of a restart tape, a displacement data plot tape and a stress data plot tape on logical units 9, 20, and 25, respectively. A small amount of additional data regarding solution and output times must be input in the format given below.

1. Solution and output times card (6F10.0)

Columns 1–10	TPRT1, first time for printed output
Columns 11–20	TPRT2, last time for printed output (also end of solution)
Columns 21–30	DTPRT, time interval for printed output
Columns 31–40	TPLT1, first time for plotted output
Columns 41–50	TPLT2, last time for plotted output
Columns 51–60	DTPLT, time interval for plotted output

C. Post-processor DFSTRW

This program creates deformed structure plots at specified times. Plots of the entire warhead or "zoomed in" plots of a specified portion can be made. The original start tape for the WHAP run and the displacement output tape for the run are read

by DFSTRW from logical units 8 and 20. Additional input data required is given below.

1. ID card (6A6)
   - Columns 2–5 — User's code
   - Columns 7–36 — User's name, phone and/or other identifying information

2. Control card (A6,4X,F10.0,3I5)
   - Columns 1–10 — ORIENT, page orientation indicator, if ORIENT = "VERTICAL---" (or blank) plots will be drawn with the Z-axis in the direction of the larger page dimension, if ORIENT = "HORIZONTAL" the axis will be in the direction of shorter page dimension
   - Columns 11–20 — SCALE, multiplication factor for displacements, if SCALE = 0. then SCALE = 1.
   - Columns 21–25 — NELI, number of first element in block to be plotted, if NELI = 0 then NELI = 1
   - Columns 26–30 — NELF, number of last element in block to be plotted, if NELF = 0 then NELF = NEL
   - Columns 31–35 — ILABEL, axis labeling indicator, if ILABEL > 0 then axes are drawn and labeled

3. Plot area card (6F10.0)
   - Columns 1–10 — RMIN, R value at left end of R-axis
   - Columns 11–20 — RMAX, R value at right end of R-axis, if RMAX – RMIN = 0. then program will determine suitable values
   - Columns 21–30 — ZMIN, Z value at lower end of Z-axis
   - Columns 31–40 — ZMAX, Z value at upper end of Z-axis, if ZMAX – ZMIN = 0. then program will determine suitable values
   - Columns 41–50 — RSTEP, R axis labeling increment, if RSTEP = 0. then RSTEP = RMAX – RMIN
   - Columns 51–60 — ZSTEP, Z axis labeling increment, if ZSTEP = 0. then ZSTEP = ZMAX – ZMIN

4. Output segments card (10I5)
   List of output segments to be plotted, at present only the first and last planes (planes 1 and MPLN) are plotted and must be specified.

5. Time cards (F10.0, one for each plot desired)
   - Columns 1–10 — T, time, if T < 0. then plot of undeformed structure will be produced

D. Post-processor CNTRW

This program creates stress contour plots at specified times. Plots of the entire warhead or "zoomed in" plots of a specified portion can be made. The original tape

for the WHAP run and the stress output tape for the run are read by CNTRW from logical units 8 and 25. Additional input data required are given below.

1. ID card (6A6)
   - Columns 2–5 — User's code
   - Columns 7–36 — User's name, phone and/or other identifying information

2. Control card (A6,4X,4I5)
   - Columns 1–10 — ORIENT, page orientation indicator, if ORIENT = "VERTICAL––" (or blank) plots will be drawn with the Z-axis in the direction of the larger page dimension, if ORIENT = "HORIZONTAL" the axis will be in the direction of shorter page dimension
   - Columns 11–15 — NELI, number of first element in block to be plotted, if NELI = 0 then NELI = 1
   - Columns 16–20 — NELF, number of last element in block to be plotted, if NELF = 0 then NELF = NEL
   - Columns 21–25 — ILABEL, axis labeling indicator, if ILABEL > 0 then axes are drawn and labeled
   - Columns 26–30 — IBND, if IBND > 0 then interior boundaries between different materials are drawn

3. Plot area card (6F10.0)
   - Columns 1–10 — RMIN, R value at left end of R-axis
   - Columns 11–20 — RMAX, R value at right end of R-axis, if RMAX – RMIN = 0. then program will determine suitable values
   - Columns 21–30 — ZMIN, Z value at lower end of Z-axis
   - Columns 31–40 — ZMAX, Z value at upper end of Z-axis, if ZMAX – ZMIN = 0. then program will determine suitable values
   - Columns 41–50 — RSTEP, R axis labeling increment, if RSTEP = 0. then RSTEP = RMAX – RMIN
   - Columns 51–60 — ZSTEP, Z axis labeling increment, if ZSTEP = 0. then ZSTEP = ZMAX – ZMIN

4. Output segments card (10I5)
   List of output segments to be plotted, at present only the first and last segments (segments 1 and MSEG) are plotted and must be specified.

5. Contour description card (3I5,3F10.0,5I5)
   - Columns 1–5 — NSIG, number indicating stress to be plotted

NSIG	Stress plotted
1	S XX
2	S YY
3	S ZZ
4	S XY
5	S XZ

6	S-YZ
7	S-HYDROSTATIC
8	S-OCTAHEDRAL

Columns 6–10	NCNTR, number of contour levels, if NCNTR = 0 or NCNTR > 10 then NCNTR = 10
Columns 11–15	JLABEL, if JLABEL ⩾ 0 then contour numerals will be connected with dashed lines
Columns 16–25	SMIN, stress value corresponding to lowest contour level
Columns 26–35	SMAX, stress value corresponding to highest contour level, if SMAX − SMIN = 0. then SMIN and SMAX will be determined by program to span values present
Columns 36–45	SSTEP, stress increment for establishing intermediate contour levels, overrides NCNTR
Columns 46–70	MATL, identification numbers of materials in which contours are to be drawn (5 maximum), if MATL(1) = 0 then contours are drawn in all materials

6. Time cards (F10.0, one for each plot desired)
   Columns 1–10 T, time

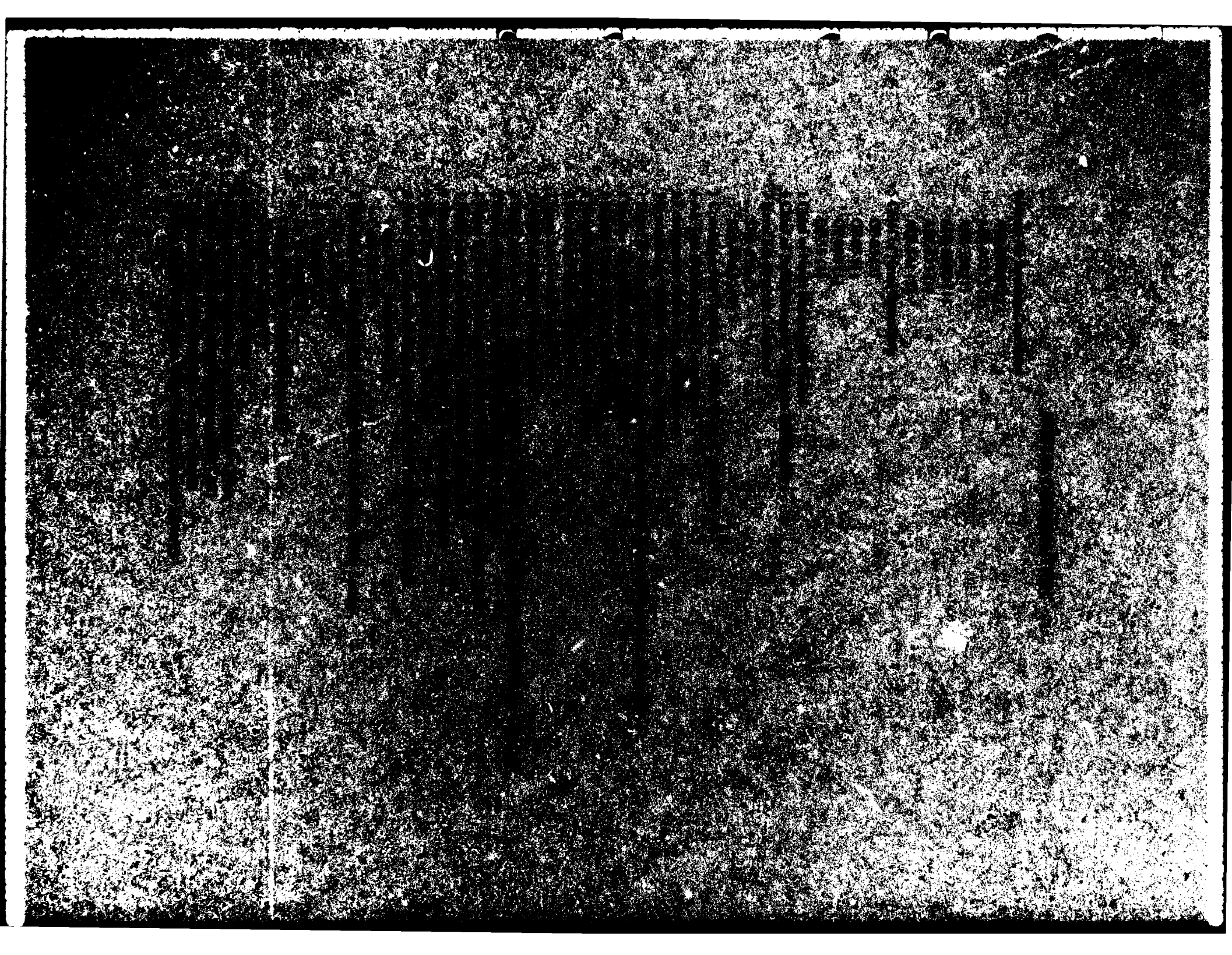

[redacted]